AD-A105 636 FOREIGN TECHNOLOGY DIV WRIGHT-PATTERSON AFB OH F/G 20/4
ACTA MECHANICA SINICA (SELECTED ARTICLES),(U)
SEP 81
UNCLASSIFIED FTD-ID(RS)T-0706-81 NL

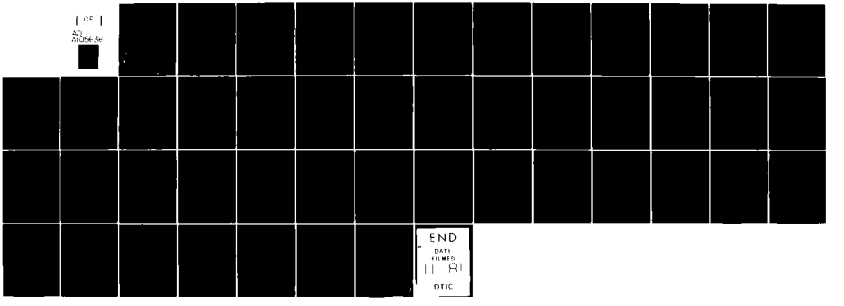

FTD-ID(RS)T-0706-81

AD A105636

FOREIGN TECHNOLOGY DIVISION

ACTA MECHANICA SINICA

(Selected Articles)

DTIC FILE COPY

1981

A

Approved for public release;
distribution unlimited.

81 10 7 168

EDITED TRANSLATION

(14) FTD-ID(RS)T-0706-81 (11) 15 September 1981

MICROFICHE NR: FTD-81-C-000844

(6) ACTA MECHANICA SINICA (Selected Articles). (12) 47

English pages: 44

Source: Acta Mechanica Sinica, Nr. 3, 1979, pp. 199-208, 266-274, 287-290

Country of origin: China
Translated by: SCITRAN
F33657-78-D-0619
Requester: FTD/TQTA
Approved for public release; distribution unlimited.

PREPARED BY:

TRANSLATION DIVISION
FOREIGN TECHNOLOGY DIVISION
WP-AFB, OHIO.

142600

TABLE OF CONTENTS

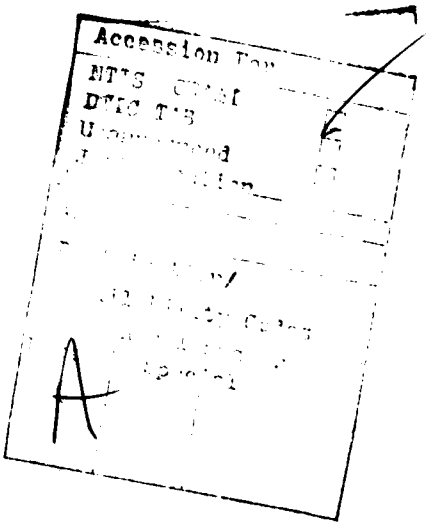

ON TRANSONIC FLOW IN HYPERBOLIC LAVAL NOZZLES*

Jia Zhen-xue, Lin Tong-ji

Abstract

Transonic flow in the throat region of hyperbolic Laval nozzles is analysed using the conformal curvilinear coordinate method. A solution to this type flow is given for the cases of different radii of wall curvature at the throat and different values of the ratio of the specific heats. The general behaviour of the transonic flow and Mach number distribution in the throat region are presented. This method gives fine accuracy. It can be applied in the designing of nozzles, especially, in the designing of aerodynamic laser nozzles.

This paper uses the conformal curvilinear coordinate method to analyze the transonic flow characteristics in the throat region of a hyperbolic Laval nozzle and gives a general solution to the transonic flow in a hyperbolic Laval nozzle. This solution is applicable to various radii of wall curvature at the throat and different ratios of specific heats. Through calculation, the relation between major parameters of the transonic flow at the throat under various specific heat ratios and radius of curvature as well as the typical Mach number distribution of the transonic flow. This method involves simple calculations and gives high accuracy. It can be used as a reference in the designing of nozzles, especially aerodynamic laser nozzles.

*Received September 10, 1977

SYMBOLS

a speed of sound, Equation (1)

b half height of the throat channel of the nozzle, Equation (1)

$f(\zeta)$ conformal curvilinear coordinate transformation function, Equation (2)

$g(\xi)$ flow related function, Equation (4)

g_s throat cross-sectional flow related function, Equation (9)

$H(\xi,\eta)$ magnification factor of the x surface relative to the ζ surface, Equations (2), (7)

M Mach number, Equation (3)

q velocity, Equation (3)

r radius of curvature of throat wall surface, Equation (7)

u velocity component in the ξ direction, Equation (3)

v velocity component in the η direction, Equation (3)

x orthogonal linear coordinate Equation (2)

y orthogonal linear coordinate Equation (2)

z complex variable of the orthogonal linear coordinate, Equation (2)

γ ratio of specific heats, Equation (4)

δ angle between the direction of the flow and the direction ξ Equation (5)

ζ complex variable of conformal curvilinear coordinates, Equation (2)

η conformal curvilinear coordinate, Equation (2)

η_b approach angle of the wall surface of a hyperbolic Laval nozzle, Equation (6)

μ Mach angle, Equation (5)

ξ conformal curvilinear coordinate, Equation (2)

ρ gas density, Equation (3)

ψ flow function, Equation (3)

ψ_s max. flux, Equation (10)

$\omega(\xi)$ function, Equation (11)

Subscripts:

$*$ critical parameters when the flow velocity equals to the local sound speed

o parameters at the center

c parameters at the points on the wall surface at the throat cross-section

s position of sound velocity point

η partial derivative with respect to η

ξ partial derivative with respect to ξ

In the design of nozzles, the dimensionless radius of curvature of the wall surface at the throat (abbreviated as the radius of curvature of wall surface at the throat) is an important parameter. It is necessary to know the relations between the maximum flow of the nozzle, the shape of the sonic speed line and flow velocity distribution in the transonic region with the radius of curvature of the wall surface at the throat. But this problem has not been solved. After selecting the radius of curvature of throat wall surface, the calculation of the corresponding velocity distribution in the transonic region to be given as the initial condition for the calculation of the supersonic section is also another problem in the design of aerodynamic laser nozzles which needs to be solved immediately.

Presently the design of nozzles primarily uses semi-empirical methods which are reliable to a certain extent when the radius of curvature of the throat wall surface is very large. But, with the reduction of the radius of curvature of the wall surface at the throat, the sonic speed line is far from a straight line. The assumption of radial flow pattern in the throat region is no longer valid. Therefore, some of the presently available methods, such as the linear sonic speed line method [1-3], the method involving the transformation of radial flow into parallel flow [4,5], etc., are no longer applicable.

As for the study of the transonic flow in the throat region of the hyperbolic Laval nozzle, some work [6-9] has been done by now which can be applied to conditions under which the radius of curvature of wall surface at the throat is larger. [10] used a time related method to calculate the special example for the flow of a hyperbolic Laval nozzle when the radius of curvature of the wall surface r is 2. Because of the introduction of the time variable and the artificial barrier term, the relation between r and the transonic flow was not given.

Considering that the transonic flow in the throat of the nozzle is primarily affected by the radius of curvature of the wall surface at the throat, this paper used the conformal curvilinear coordinate method to provide a general solution to the transonic flow in a hyperbolic Laval nozzle in a unified form. This solution is not only applicable to various radii of curvature of throat wall surface, but also to different ratio of specific heats.

I. FLOW FUNCTION RELATIONS

Let us consider the two-dimensional steady non-rotational isoentropic flow of an ideal gas. Let us use the half height of the throat b and the central parameters a and ρ as the bases to introduce some dimensionless quantities. Based on the meaning of each symbol in the table of symbols, a "-" is added over the head of each corresponding symbol:

$$\bar{x} = x/b,\ \bar{y} = y/b,\ \bar{r} = r/b,\ \bar{u} = u/a_0,\ \bar{v} = v/a_0,\ \bar{\rho} = \rho/\rho_0,\ \bar{\psi} = \psi/a_0\rho_0 b \quad (1)$$

The discussion in this paper uses dimensionless quantities. For convenience, the "-" sign over the symbol is omitted. Let x,y be the orthogonal coordinates on a physical plane and ξ,η be the curvilinear coordinates which have a conformal relation with x,y. Based on the theory of the complex function, there are the following relations between the coordinates mentioned above:

$$z = f(\zeta),\ z = x + iy,\ \zeta = \xi + i\eta,\ H(\xi,\eta) = |dz/d\zeta| \quad (2)$$

when $H(\xi,\eta)$ is defined as the magnification factor of the z plane relative to the ζ plane. Based on the definition of the flow function $\psi(\xi,\eta)$ and the isoentropic relation of the flow, the velocity components u, v in the ξ,η directions, density ρ and Mach number M have th following relation with the flow function ψ [11]:

$$\left.\begin{aligned} &u = \psi_\eta/\rho H,\ v = -\psi_\xi/\rho H,\ q^2 = u^2 + v^2 \\ &\rho^{(\gamma+1)} - \frac{\gamma+1}{2}\rho^2 + \frac{\gamma-1}{2H^2}(\psi_\xi^2 + \psi_\eta^2) = 0 \\ &M = q\left(\frac{\gamma+1}{2} - \frac{\gamma-1}{2}q^2\right)^{-\frac{1}{2}} \end{aligned}\right\} \qquad (3)$$

Let us consider that the streamline of a compressible flow in the nozzle is approximately the same as that of an incompressible flow. When the streamline and the equipotential line of the incompressible flow are chosen as the conformal curvilinear coordinates ξ and η, then the velocity component $|u| >> |v|$. From the first equation in (3), we have $|\psi_\eta| >> |\psi_\xi|$. Using this condition, as an approximation, we are going to neglect all the terms containing the small quantity ψ_ξ in the flow function under the conformal curvilinear coordinates to obtain a simplified equation for the flow function under the conformal curvilinear coordinates. The solution to this simplified flow function has the following integral form [11]:

$$\psi(\xi, \eta) = \left(\frac{\gamma+1}{2}\right)^{\frac{1}{\gamma-1}} g(\xi) \int_0^\eta \left[1 - \frac{\gamma-1}{\gamma+1}\frac{g^2(\xi)}{H^2(\xi,\eta)}\right]^{\frac{1}{\gamma-1}} d\eta \qquad (4)$$

where $H(\xi,\eta)$ is a known function of the chosen coordinates (ξ,η), $g(\xi)$ is a function to be determined by the boundary conditions. For convenience, $g(\xi)$ is called the flow related function.

In the curvilinear coordinate system ξ,η which has a conformal relation with the orthogonal linear coordinates x,y, the forms of the equations of characteristic lines are invariant. It can be written as:

$$\frac{d\xi}{d\eta} = \operatorname{ctg}(\theta \pm \mu),\ \theta = -\operatorname{tg}^{-1}(\psi_\xi/\psi_\eta),\ \mu = \sin^{-1}(1/M) \qquad (5)$$

Based on custom, the "+" in Equation (5) represents the first family of characteristic lines and "-" represents the second family of characteristic lines. Thus, from Equation (5) we can calculate the influence line which is the second family characteristic line that passes through the wall surface point at the cross-

section of the throat. The extremum characteristic line is the second family characteristic line which passes through the sonic speed point on the center line. The branch line is the first family characteristic line which passes through the sonic speed point on the center line [11]. Notice that δ,μ and M in Equation (5) are all functions of the flow function $\psi(\xi,\eta)$.

II. TRANSONIC SOLUTION OF THE NOZZLE

The solution of an incompressible potential flow in a hyperbolic nozzle is [12] $z = \csc\eta_b \operatorname{sh}\zeta,\ z = x + iy,\ \zeta = \xi + i\eta$ (6)

where the coefficient $\csc \eta_b$ is to make b be 1. Let us separate the real and the imaginary parts of Equation (6) to obtain the relations between the orthogonal linear coordinates x,y and the curvilinear coordinates ξ,η. Through the use of differential geometry and the definition of $H(\xi,\eta)$ in Equation (2), we obtain the expressions for the radius of curvature of the wall surface at the throat and the magnification factor $H(\xi,\eta)$, respectively, as:

$$x = \csc\eta_b \operatorname{sh}\xi\cos\eta,\ y = \csc\eta_b \operatorname{ch}\xi\sin\eta,\ r = \operatorname{ctg}^2\eta_b,\ H(\xi,\eta) = \csc\eta_b(\operatorname{sh}^2\xi + \cos^2\eta)^{\frac{1}{2}} \quad (7)$$

From the third equation in (7), we can see that corresponding to different η_b we can get a series of different hyperbolic nozzles shown in Figure 5. Substituting $H(\xi,\eta)$ into Equation (4), we get the solution of the flow function $\psi(\xi,\eta)$ of the hyperbolic nozzle as

$$\psi(\xi,\eta) = \left(\frac{\gamma+1}{2}\right)^{\frac{1}{\gamma-1}} g(\xi)\int_0^{\eta}\left[1 - \frac{\gamma-1}{\gamma+1}g^2(\xi)\sin^2\eta_b/(\operatorname{sh}^2\xi+\cos^2\eta)\right]^{\frac{1}{\gamma-1}} d\eta \quad (8)$$

when $\xi = 0$ and $\eta = \eta_b$, Equation (8) gives the flow ψ_b passing through the cross-section of the throat. At this time, ψ_b is only a function of g(0). In the supersonic flow in the nozzle, ψ_b should satisfy the condition of the maximum cross-sectional flow at the throat, i.e., $[\partial\psi_b/\partial g(0)] = 0$ [11]. Therefore, from Equation (8) we get

$$\int_0^{\eta_b} [1 - g^2(0)\sin^2\eta_b \sec^2\eta] \left[1 - \frac{\gamma-1}{\gamma+1} g^2(0)\sin^2\eta_b \sec^2\eta\right]^{\frac{2-\gamma}{\gamma-1}} d\eta = 0 \tag{9}$$

where g(0) has multiple values. The minimum real positive root is the flow related function of supersonic flow in the nozzle which is expressed as g_s. From Equation (8), we can get the selected η by substituting g_s into it and letting $\xi = 0$ and the upper limit of the integral $\eta = \eta_b$. This is the maximum flow ψ_s corresponding to the selected r.

Based on the boundary condition s, when $\eta = \eta_b$, $\psi_b = \psi_s$. Let us bring this relation into Equation (8) and obtain the relation to determine the flow related function $g(\xi)$ of supersonic flow in nozzles:

$$\left(\frac{\gamma+1}{2}\right)^{\frac{1}{\gamma-1}} g(\xi) \int_0^{\eta_b} \left[1 - \frac{\gamma-1}{\gamma+1} g^2(\xi)\sin^2\eta_b/(\mathrm{sh}^2\,\xi + \cos^2\eta)\right]^{\frac{1}{\gamma-1}} d\eta = \psi_s \tag{10}$$

In Equation (10), $g(\xi)$ has multiple values. For a given ξ, the choice of $g(\xi)$ is as follows: when $\xi < 0$, $g(\xi)$ is the minimum positive real root corresponding to the flow in the contraction region; when $\xi = 0$, $g(\xi)$ is the minimum real multiple root corresponding to the cross-sectional flow at the throat; when $\xi > 0$, $g(\xi)$ is the second real positive root corresponding to the flow in the expansion region [11].

Based on Equations (3), (5), (7)-(10) and by choosing $\gamma = 1.4$, this paper has calculated the flow characteristics of several conditions with r equal to 10.6, 5, 2.1, 0.5 and 0.22 respectively. In addition, the Mach number distributions, influence line, extremum characteristic line and branch line under the conditions that r is 2 and γ is 1.667, 1.4 and 1.2 are also calculated. The results are shown in Sections 4-9.

Besides, the condition that γ is 2 corresponds to the simulated gas motion using the free surface flow of water [13]. Under this

condition, based on Equation (8), the flow function $\psi(\xi,\eta)$ can be integrated into the following simple analytical expressions:

$$\left.\begin{aligned}\psi(\xi,\eta) &= \frac{3}{2}\eta g(\xi) - \frac{1}{2}\sin^3\eta_b \operatorname{csch} 2\xi \operatorname{tg}^{-1}(\operatorname{th}\xi \operatorname{tg}\eta) g'(\xi)\\ g(\xi) &= [2\csc\eta_b(\eta_b \operatorname{ctg}\eta_b)^{\frac{1}{3}}/\omega(\xi)]\cos\frac{1}{3}[\pi \pm \cos^{-1}\omega(\xi)]\\ \omega^3(\xi) &= 2\operatorname{ctg}\eta_b \operatorname{csch} 2\xi \operatorname{tg}^{-1}(\operatorname{th}\xi \operatorname{tg}\eta_b)\end{aligned}\right\} \qquad (11)$$

Under such conditions, the maximum flow ψ_s, the cross-sectional flow related function g_s at the throat, the wall surface point velocity $q(0,\eta_b)$ on the cross-section at the throat and the center point velocity $q(0,0)$ have the following simple relations with r:

$$\begin{aligned}\psi_s &= r^{\frac{1}{3}}(1+r)^{\frac{1}{3}}(\operatorname{ctg}^{-1}r^{\frac{1}{3}})^{\frac{1}{3}}\\ g_s &= r^{\frac{1}{3}}(1+r)^{\frac{1}{3}}(\operatorname{ctg}^{-1}r^{\frac{1}{3}})^{\frac{1}{3}}\\ q(0,\eta_b) &= r^{-\frac{1}{3}}(1+r)^{\frac{1}{3}}(\operatorname{ctg}^{-1}r^{\frac{1}{3}})^{\frac{1}{3}}\\ q(0,0) &= r^{\frac{1}{3}}(\operatorname{ctg}^{-1}r^{\frac{1}{3}})^{\frac{1}{3}}\end{aligned} \qquad (12)$$

III. MAXIMUM FLOW

The flow discussed in the section is the dimensionless flow expressed by the critical parameters ρ_*, a_* and the half height of the throat channel b. It is also generally called the flow coefficient. For nozzles with a given wall surface pattern, because of the limitation of the cross-section at the throat, there is a maximum flow value permitted to pass through the cross-section of the throat which is the maximum flow ψ_s. The maximum flow ψ_s is an important parameter of nozzle flow and it is a necessary condition of supersonic flow in the nozzle. It is also the necessary condition for the assurance of the continuous transfer from subsonic to supersonic in the transonic flow in the throat region. In the study of the transonic flow in the nozzle, there has been no good solution to the problem of the maximum flow passing through the cross-section at the throat. For example, in the relaxation iteration method, because the maximum flow ψ_s is not determined, it was assumed to be 1 [14]. This assumption can only be applied

approximately when r is large. [9] gave the maximum flow in the form of an infinite series which has poor convergence and it showed vibration.

This paper carried out calculations based on Equations (8) and (9). In Figure 1 the curves of the maximum flow ψ_s are shown versus r when γ is 1.2, 1.4 and 2.0, respectively. From the figure, it was found that when r is larger and approaching 1, ψ_s is basically not affected by γ at this time. With decreasing r, ψ_s becomes smaller. For example, when γ is 1.4, r = 1.0, ψ_s = 0.987; r = 0.50, ψ_s = 0.970; γ = 0.1, ψ_s = 0.883. For a given r, if γ increases, then ψ_s is decreased. The smaller r is, the larger the effect of γ on ψ_s.

IV. SONIC SPEED LINE

Sonic speed line is the boundary line between the subsonic region and supersonic region in the transonic flow. It is also the intersection of the elliptical equation and the hyperbolic equation. Therefore, the determination of the shape and position of the sonic speed line has always been the major point in the study of transonic flow in the nozzle.

Based on Equations (9)-(11), Figure 2 gives curves showing the relation between the sonic speed point position y_s and r for the conditions when γ is 1.2, 1.4 and 2.0, respectively. y_s decreases with increasing γ which is that with increasing r the position of the sonic speed point at the cross-section of the throat moves towards the center line. When γ increases, then y_s also increases which means that the position of sonic speed point at the cross-section of the throat moves towards the wall surface.

Figure 3 gives the curves showing the relation between the sonic speed points on the wall surface as well as on the center

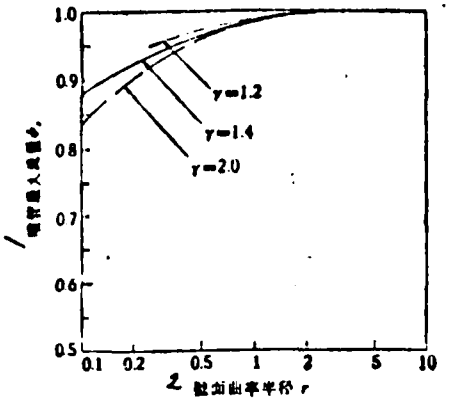

FIGURE 1. Relation between max. flow and radius of curvature

Maximum flow of nozzle ψ_s			
r \ γ	1.2	1.4	2.0
1.0	0.9890	0.9874	0.9841
2.0	0.9961	0.9957	0.9946

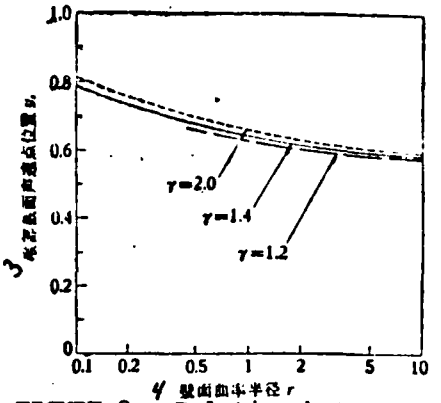

FIGURE 2. Relation between sonic speed point with radius of curvature I

Key: 1--maximum flow of the nozzle ϕ; 2--radius of curvature of wall surface r; 3--position of sonic speed point at the cross-section of throat y; 4--radius of curvature of wall surface r

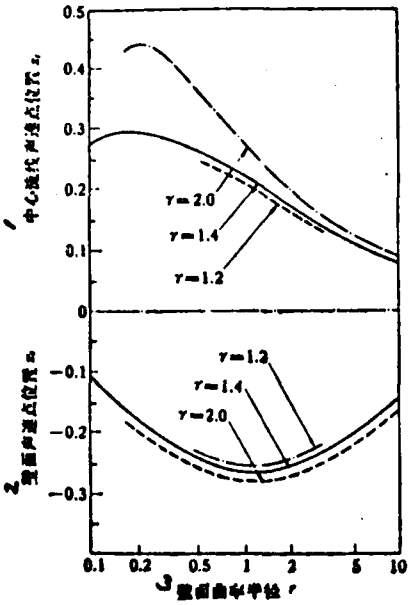

Figure 3. Relation between sonic speed point and radius of curvature II

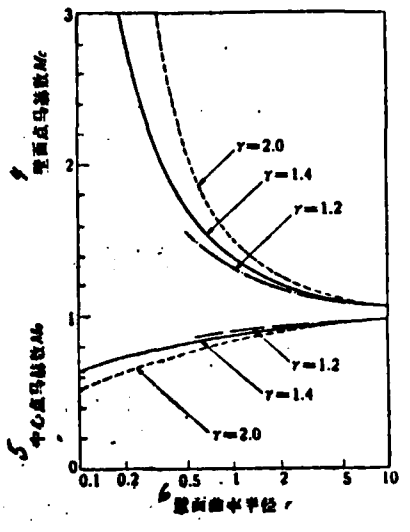

Figure 4. Relation between Mach number at the cross-section at the throat and radius of curvature

Key: 1--position of sonic speed point on center streamline x_1; 2--position of sonic speed point on wall surface x; 3--radius of curvature of wall surface r; 4--Mach no. at wall surface point Mc; 5--Mach no. at center point Mo; 6--radius of curvature of wall surface r.

line with r when γ is 1.2, 1.4 and 2.0 respectively. The sonic speed point on the wall surface is located upstream to the cross-section of the throat, i.e., $x_s < 0$. When γ is 1.4, $|x_s|$ has a maximum value of 0.267 at r = 1.1. With increasing γ, the sonic speed point on the wall surface moves upstream(that is the value of $|x_s|$ increases). The sonic speed point on the center line is located downstream to the cross-section of the throat, i.e., $x_s > 0$. When γ is 1.4, x_s has a maximum of 0.295 at γ = 0.18. With increasing γ, the position of the sonic speed point on the center line moves downstream.

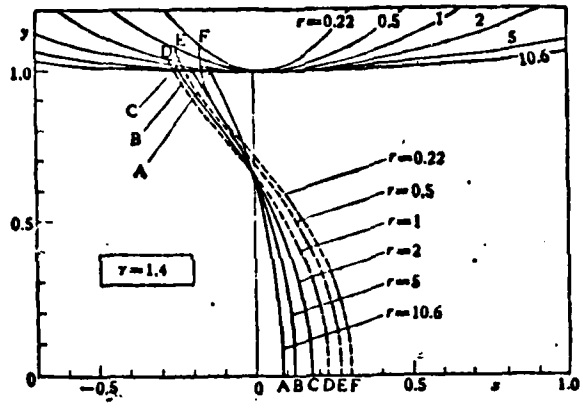

Figure 5. The shapes of the sonic speed lines

Figure 5 shows the shapes and positions of the sonic speed lines under the conditions that r is 1.4 and γ is 10.6, 5.0, 2.0, 1.0, 0.5 and 0.22 respectively. From the figure, it shows that when r > 1.1, there is only a turning point on the center line. But when r < 1.1, there is another turning point appearing near the wall surface. With decreasing r, the curvature of the sonic speed line becomes larger. Referring to Figure 3, it can be found that the variation of the absolute value of the position of the sonic speed x_s on the wall surface. Starting from r = 10.6, $|x_s|$ gradually becomes larger. When r = 1.1, $|x_s|$ has the maximum value. When r continues to decrease, $|x_s|$ gradually becomes smaller. Another turning point appears near the wall surface. In the range where the sonic speed lines were plotted in Figure 5, the position

of the sonic speed point on the center line x_s monoclinically decreases with increasing r.

V. FLOW VELOCITY AT THE CROSS-SECTION OF THE THROAT

In the flow in a nozzle, the flow velocity distribution at the cross-section of the throat is mainly affected by r and γ. When r is very large, the gas flow velocity can approach the sonic speed at the cross-section of the throat. But with decreasing r, the inhomogeneity of the flow at the throat rapidly increases. The linear sonic speed line assumption [2] is no longer applicable.

Figure 4 shows the curves showing relations between the Mach numbers at the center point on the cross-sectional surface of the throat as well as at the wall surface point with r when γ is 1.2, 1.4 and 2.0, respectively. From this figure, it can be seen that $M_c < 1$ and $M_o > 1$. The smaller r is the larger the difference between M_o and M_c becomes. The increase in γ causes further inhomogeneity of the distribution of Mach number at the cross-section of the throat and the difference between M_o and M_c increases.

VI. FLOW VELOCITY OF THE CENTER LINE

In order to explain how r can quantitatively influence the flow velocity distribution on the center line of the nozzle, Figure 6 gives the Mach number distributions for the conditions that γ is 1.4 and r is 10.6, 5.0, 2.0, 1.0, 1.5 and 0.22, respectively. The figure shows that when x is approximately 0.37, for different r all the center line Mach number distribution curves intersect approximately at one point. The Mach number M at this point is 1.08. This intersection point is the turning point of the center line Mach number distribution curves. Near this turning point, the acceleration of the flow is the fastest. The distribution of the Mach number near the turning point is approximately a straight line.

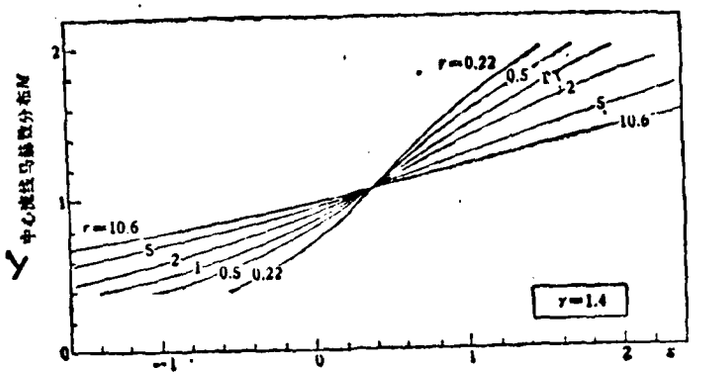

Figure 6. Center line Mach number distribution
Key: 1--distribution of center streamline Mach Number M

The larger r is, the approximate straight line region is also larger. When r decreases, the slope of the approximately straight line increases which is that the acceleration of the flow increases.

VII. TRANSONIC FLOW

Based on Equations (8)-(10), we obtain the transonic flow in the throat region. The results are shown in Figures 7-10. When r is larger, the distribution of the equi-Mach number line in the throat region is relatively homogeneous. With decreasing r the curvature of the Mach number line becomes more severe and the more inhomogeneous the distribution of the flow velocity in the flow field becomes. The smaller r is, the more concentrated near the wall surface at the throat the acceleration of the gas flow becomes and the flow velocity near the center point becomes slower.

Figure 8 shows the equi-Mach line distribution in the throat region of a hyperbolic nozzle where γ is 1.4 and r is 2. As a comparison, in the same figure, the results of Cherry [8] and Serra [10] are also plotted. Cherry used a potential iteration method to obtain the precise solution of flow in the nozzle with an approximate hyperbolic wall surface for $\gamma = 1.4$ and $r = 2$, and Serra used

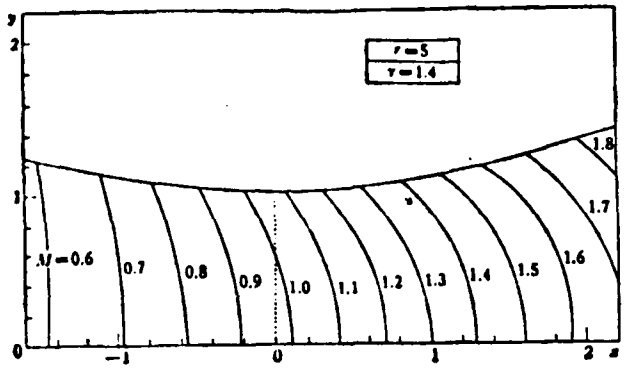

FIGURE 7. Equi-Mach number line distribution at the throat of the nozzle.

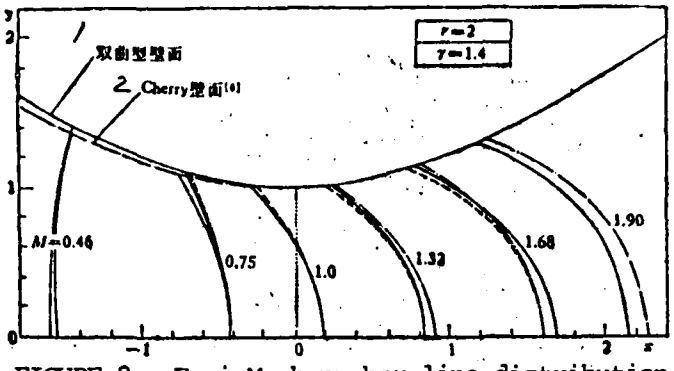

FIGURE 8. Equi-Mach number line distribution at the throat of the nozzle.
——this paper — . —Cherry [8] – –Serra [10]

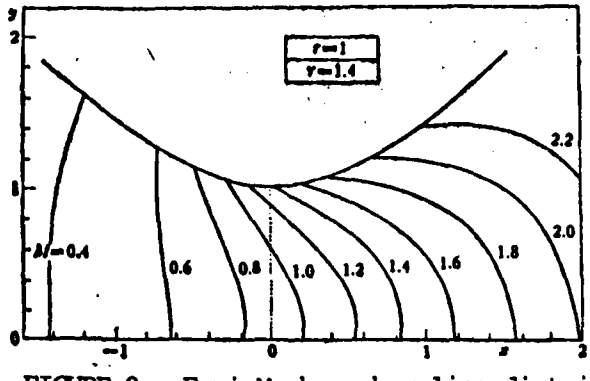

FIGURE 9. Equi-Mach number line distribution at the throat of the nozzle.

Key: 1--hyperbolic wall surface; 2--Cherry wall surface

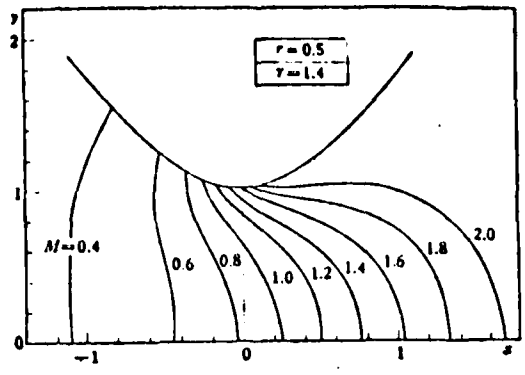

Figure 10. Distribution of Equi-Mach number line at the throat of the nozzle

a time related method to obtain the distribution of equi-Mach number line in the throat region of a hyperbolic nozzle when γ is 1.4 and r is 2. From Figure 8, it was found that the results of sonic speed line in this work coincide with those obtained by Cherry. For the equi-Mach lines when M is 0.46 and 1.90, our results agree with results of Serra. When M is 0.75, 1.32 and 1.68, our results are situated between the results of Cherry and Serra.

VIII. THE EFFECT OF γ

In order to study the effect of γ on the flow in the nozzle, we carried out calculations corresponding to the situation that γ is 1.2, 1.4, 1.667 and 2.0, respectively. Figure 1 shows the relation between the maximum flow ψ_s with r under different γ. The results indicate that when γ increases, ψ_s decreases. When r is larger, the effect of γ on ψ_s is small. When r is larger, it can be approximately considered that ψ_s is not affected by γ. From Figures 2 and 3, it can be found that when γ increases, the sonic speed point on the cross-sectional surface at the throat is moving towards the wall surface and the positions of the sonic speed point on the wall surface and the center line move toward upstream and downstream, respectively. That means the absolute value of x_s is increasing.

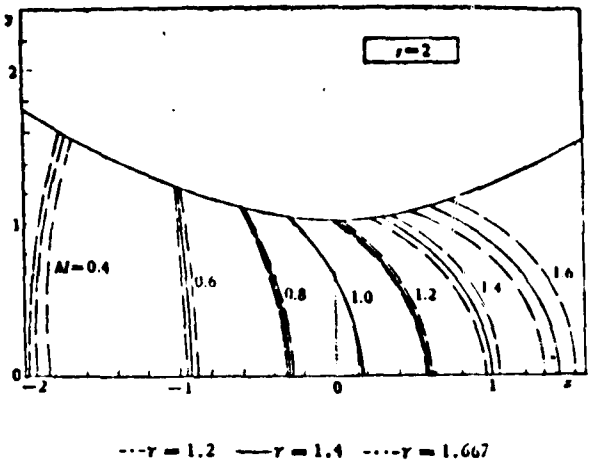

Figure 11. The effect of ratio of specific heats on the equi-Mach number line

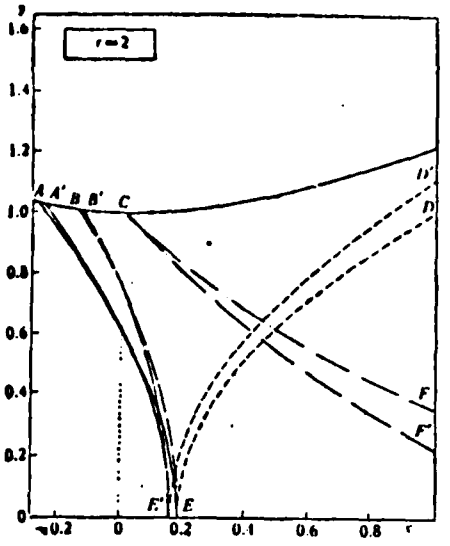

Figure 12. The effect of ratio of specific heats on the flow at the throat

Key: 1--name; 2--line pattern; 3--sonic speed line; 4--extremum characteristic line; 5--influence line; 6--branch line

1名称	2图例	γ = 1.667	γ = 1.2
3声速线	——	AE	A'E'
4极限特征线	—·—·—	BE	B'E
5影响线	—··—··	CF	CF'
6分支线	————	DE	D'E'

From Figure 4, it can be found that M increases but M decreases with increasing γ. This means that the increase in γ makes the distribution of Mach number across the cross-section at the throat inhomogeneous. When r is smaller, the effect of γ is larger. When r is larger, the effect of γ is smaller. From Figure 11, we can see that, with increasing γ, the equi-Mach number lines both upstream and downstream move towards the throat region. In addition, as the flow speed approaches the sonic speeds, the displacement gradually decreases. The effect of γ on the shape and position of the sonic speed line is small. Figure 12 shows the r=2 positions of the sonic lines, influence lines, extremum characteristic lines and branch lines when γ is 1.2 and 1.667. The variation of γ has very small effect on the shape and position of the sonic speed lines and the extremum characteristic lines but it has a large effect on the influence lines and branch lines. The

influence region increases with increasing γ which is located inside the expansion section. The increase in this region is not affected by the streamline pattern of the wall surface in the expansion section.

IX. CONCLUSIONS

This paper used the conformal curvilinear coordinate method to analyze the characteristics in the transonic flow region of hyperbolic Laval nozzles and gave a general solution in a unified fashion to the transonic flow in hyperbolic nozzles. This solution is not only applicable to various radii of curvature of the wall surface at the throat but also to different ratios of specific heats. Through calculations, we obtained the typical curves of the variations of the characteristics of the transonic flow at the throat with the radius of curvature of the wall surface at the throat under different ratios of specific heats. It included the maximum flow in the nozzle, sonic speed line and the Mach number distribution on the center line, etc. It also gave the transonic flow at the throat with typical radius of curvature of the wall surface.

We have carried out a comparison between our result and those obtained by Cherry [8] and Serra [10]. The nozzles they discussed correspond to the same situation as r is 2 and γ is 1.4 in this paper. The results indicated that there is good agreement in terms of equi-Mach number lines. This explains that in addition to the capability of selecting the radius of curvature of the wall surface at the throat based on the need and of adjusting the ratio of specific heats r, as well as ease of calculation, the conformal curvilinear coordinate method has fairly high accuracy.

REFERENCES

[1] Puckett, A. E., *J. Appl. Mech.*, 13, 4 (1946), A265—A270.

[2] Greenberg, R. A., Schneidermans, A. M., Ahouse, D. R. and Parmentier, E. M., *AIAA. J.*, 10, 11 (1972), 1494—1498.

[3] Полежаинна, Н. А. и Шифрин, Э. Г., *Изв. АН СССР, МЖГ*, 1 (1975), 54—58.

[4] Atkin, A. O. L., Two-Dimensional Supersonic Channel Design Part I, ARC RM 2174 (1945).

[5] Dumitrescu, L. Z., *AIAA J.*, 13, 4 (1975), 520—521.

[6] Oswatitsch, K. und Rothstein, W., Das Strömung in einer Lavaldüse, Jb. dtsch Lufol, 91—103 (1942), Transl. as NACA TM—1215.

[7] Emmons, H. W., The theoreticalstudy of a fractionless, adiabatic, perfect gas inside of two-dimensional hyperbolic nozzle, NACA TN—1003 (1946).

[8] Cherry, T. M., *J. Australian Math. Soc.*, 1 (1959), 80—94.

[9] Hall, I. M., *The Quart. J. of Mech. and Appl. Math.*, 15, Part 4 (1962), 487—508.

[10] Serra, R. A., *AIAA J.*, 10, 5 (1972), 603—621.

[11] Lin Tung-Chi and Jar Cheng-Sho, Acta Mechanica Sinica, 1 (1978) pp 1-18.

[12] Lamb, H., Hydrodynamics, Sixth Edition, New York (1945), 73—74.

[13] Riabouchinsky, D., Mécanique des Fluides, *Comptes Rendus Acad. Sci. Paris*, 195, 22 (1932), 998—999.

[14] Fox, L. and Southwell, R. V., *Proc. Roy. Soc.*, (A)183 (1944), 38—54.

[15] Kliegel, J. R. and Levine, J. N., *AIAA J.*, 7, 7 (1969), 1375—1378.

EXPERIMENTAL TECHNIQUE AND EXPERIMENTAL METHOD

COMPRESSION PROCESSES OF FREE PISTONS AFTER THE OPENING OF NOZZLE IN A HYPERSONIC GUN TUNNEL * 1)

Qian Fu-xing, Xiao Lin-kui, Shi Zhen-ping
Institute of Mechanics, Academia Sinica

ABSTRACT

The report is concerned with compression processes of free pistons after the opening of nozzle in a hypersonic gun tunnel. The nozzle flow will start at the time when the primary shock running ahead of the piston reaches the diaphram at the entrance of the nozzle and the piston starts to decelerate at the time when the shock reflected from the nozzle strikes it. The momentum equation for the motion of the piston and the continuity equation of mass of the gas are derived respectively, and the finite-difference calculations are carried out by computers.

According to the results obtained, piston deceleration, overrush, rebound, oscillations, equillibrium running and peak pressure are discussed for various given initial conditions. It is shown that compression processes of free pistons after the opening of nozzle in a hypersonic gun tunnel are significantly different from those for a closed nozzle. The results are compared with those obtained with equilibrium technique based on closed nozzle and with some experimental data, and furnish important information for the operation of hypersonic gun tunnels.

* Received November 21, 1978.

1) This paper has been presented in the First National Shock Wave Conference of the Institute of Mechanics, November 12, 1978.

This paper considers the compression processes of free pistons after the opening of the nozzle in a gun tunnel and establishes the equation of motion of the piston and equation of flows in the nozzle. Furthermore, it uses the finite difference method and an electronic computer to carry out a calculation. Based on the cal= culated results, it discusses the related problems, such as the overrush, rebound, oscillation, equilibrium running and peak pressure, etc., of the piston after the opening of the nozzle under various initial conditions. These results are compared with those obtained with the conventional equilibrium piston running technique based on closed nozzle and with some experimental results and furnished some meaningful reference data for the operation of gun tunnels.

SYMBOLS

a_i -- speed of sound in region i (i=1,2,3,4,5, represent the various regions in Figure 1 same below)

a_F -- speed of sound in the rear region when the piston is in equilibrium

A -- cross-sectional area of the driven section (cm^2)

A* -- cross-sectional area of the throat passage of the nozzle (cm^2

g -- gravitational acceleration

M -- mass of the piston (kg)

M_e -- equilibrium piston mass (kg)

M_s -- Mach number of the main shock wave

P_A, P_B, P_e, P_i - represent the gas pressure in front of the pis- ton, behind the piston, in equilibrium and in region i, respectively (kg/cm^2)

$\hat{p}$ -- peak pressure (kg/cm^2)

S -- main shock wave

S_{r_1} -- reflected shock wave

t -- time

T_i -- temperature in region i (°K)

u_f -- equilibrium piston velocity, also the flow velocity in the stationary chamber in equili- brium

u_i -- flow velocity in region i

u_p -- piston velocity in uniform motion

u_{p_K} -- velocity at the point the pis- ton starts to decelerate

x -- length coordinate which orig- inates at the entrance of the nozzle (Figure 1)

X_k -- x coordinate at the time the piston starts to decelerate

ρ - gas density

γ - experimental gas ratio of specific heats

I. INTRODUCTION

Figure 1 is the trajectory of the piston motion in an equi-cross-section hypersonic gun tunnel and the x-t wave series diagrams. When a diaphram breaks, the high pressure drives the gas to suddenly make the stationary piston to accelerate and move rapidly forward along the driven section. After a period of accelerated motion, the piston reaches the maximum velocity and enters the uniform motion state. In the accelerating process, a series of compressed wave is formed in front of the piston. They further concentrate and form the main shock wave S. The shock wave S moves toward the inlet of the nozzle at a velocity higher than that of the piston. When it reaches the entrance of the nozzle, it on one hand breaks the secondary diaphram which seals the inlet to make the experimental gas to begin flow into the experimental section through the nozzle. On the other hand, it is simultaneously reflected at the entrance of the nozzle. The shock waves which follow are repeatedly reflected between the piston and the nozzle entrance. When the first reflected shock wave S_{r_1} meets the piston, it forces the piston to decelerate. But because the piston has a certain kinetic energy, it still moves forward. In the process of repeated reflection of shock waves, under general conditions the piston will "oscillate" near the end of the tube which is the oscillation motion. It also produces a high pressure peak $\hat{p}$ in the experimental gas. Only after damping over a certain period of time, the oscillation will disappear. Afterwards, it reaches a stable equilibrium state. The pressure of the experimental gas is P_e. The pressure peak $\hat{p}$ and equilibrium pressure P_e of the experimental gas as well as the corresponding temperature rise are produced due to the adiabatic compression of the piston and the non-isoentropic compression of multiple shock waves. In the piston decelerating process, a series of compressed waves is produced in the driving gas behind it. They will concentrate to form a reverse shock wave S_R which moves towards the driving section.

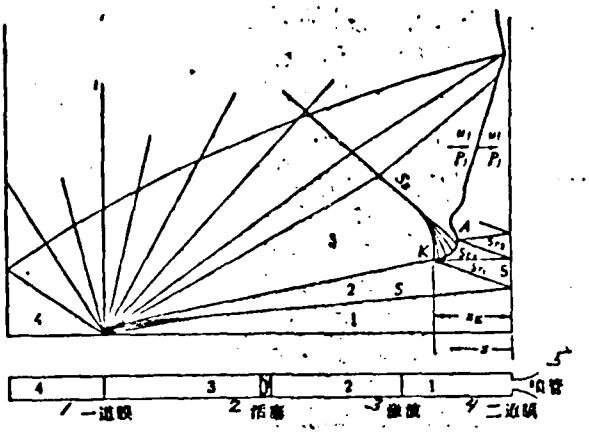

Figure 1. Trajectory of piston motion and wave series
1--primary diaphram; 2--piston; 3--shock wave; 4--second diaphram; 5--nozzle

In the developmental process of the hypersonic gun tunnel, piston motion dynamics has attracted a lot of research interests both theoretically and experimentally. The work performed in this field has been described in detail in [1-5]. But all those studies were carried out under the condition that the nozzle is not open. Actually, as described above, when the main shock wave reaches the entrance of the nozzle it breaks the secondary diaphram and starts the flow in the nozzle. However, these studies did not consider the effect of the flow in the nozzle or the piston compression processes. *神元五郎等 et al.,[6,7], measured the trajectory of the piston motion using the microwave technique and obtained the following under the conditions with and without the flow in the nozzle. Under the same initial conditions, the flow in the nozzle has a relaxing action on the overrush of the piston. Knöös [8] theoretically treated the isoentropic compression processes which make the driving gas in front of the piston reach the peak pressure in the driving section of the shock tube in a free piston drive. The analytical results indicate that the sonic speed hole at the primary diaphram has a relaxation reaction to the motion of the piston under certain conditions. But the hypersonic gun tunnel situation is completely different because the gas in front of the

*Japanese names

piston of the gun tunnel has the non-isoentropic processes due to the presence of shock waves. In addition, in the treatment of Knöös the pressure of the driving gas behind the piston can be neglected. It cannot be neglected for gun tunnels. It is especially true when using the equilibrium piston technique.

This paper will attempt to treat this problem theoretically by considering the compression processes of the free pistons after the opening of the nozzle in a gun tunnel and then to establish the related equations and followed by choosing some typical conditions to carry out a computational analysis in order to explain the effect of the existence of the flow in the nozzle on the compression processes of the piston and other relented parameters. In the meantime, the calculated results are compared with some experimental results to obtain some meaningful conclusions.

II. COMPRESSION PROCESSES OF FREE PISTONS AFTER THE OPENING OF THE PISTON IN A HYPERSONIC GUN TUNNEL

From the above description, it can be found that in a gun tunnel from the start to shut-down the piston has experienced the processes of acceleration, uniform velocity, deceleration and oscillation as well as reaching the equilibrium state. From the instance that the primary reflected shock wave S_{r_1} meets the piston and make it decelerate, the motion of the piston may have the following two conditions: 1) because the piston has a relatively large kinetic energy, the piston may overrush to a distance very close to the entrance of the nozzle to produce an extremely high peak pressure. It then rebounds, oscillates and finally reaches the equilibrium state; 2) if the mass of the piston, the ratio of the initial pressures in the driving and driven section and initial parameters, such as A^*/A can be properly selected, the piston may not have overrushing and oscillation and it may stably enter the equilibrium state. In the equilibrium state, the pressures on

both sides of the piston are equal. The piston moves at a uniform velocity u_p, which is determined by the steady flow in the nozzle towards the inlet of the nozzle. Under this condition, the peak pressure is eliminated and the experimental time is lengthened. This is the equilibrium piston technique in considering flow in the nozzle. The gun tunnel should avoid the first situation to the extent possible and attempt to operate under the second condition.

As described above, the experimental gas in front of the piston has experienced non-isoentropic compression by multiple shock waves before reaching an equilibrium state. Also in the piston deceleration process, there is a series of expansion waves originating from in front of the piston. These expansion waves will surpass the shock waves reflected from the piston. Besides, due to the deceleration of the piston, the pressure behind the piston is also varying. All these make the analysis become more complicated.

The following is a consideration of these factors in sequence. The analysis by Evans et al.[9] and Winter has already indicated that after being compressed by the third order shock wave s_{r_3} or the fourth order shock wave s_{r_4} the entropy of the experimental gas can be neglected. However, in reality as Stalker [1] has analyzed that by neglecting the entropy variation after s_{r_4} only very small error is created. In addition, Courant and Friedricks verified through calculation of a real example that because the sonic speed of the gas behind the third order shock wave s_{r_3} is higher, when the expansion waves in front of the piston surpass that shock wave, it is drastically reduced to near the Mach wave. Therefore, we treat the first and second order shock wave compressions of the experimental gas as non-isoentropic processes but consider the variation of the state of gas after it (i.e., after region (5)) approximately as isoentropic processes. Therefore, the pressure in front of the piston can be written as

$$P_4 = P_3(\rho/\rho_3)^\gamma \qquad (1)$$

As for the pressure variation behind the piston, we can make this analysis. In the deceleration process, the slope of the compression wave $(dt/dx = 1/(u - a))$ produced behind the piston becomes steeper and finally it forms an enveloping curve. When the deceleration of the piston is constant, this enveloping curve is a parabolic curve which is the shock wave curve formed behind the piston. Its starting point is located on the negative characteristic line created at the beginning of the deceleration of the piston. The larger the deceleration, the closer this starting point of the enveloping curve is to the starting point of deceleration. In the piston deceleration process, its back pressure is determined by the motion of the piston and the compression generated by it. Therefore, when shock waves occur in this series of waves, it is not possible to find closed solutions to the motion. Let us assume that at any instance this pressure is equal to the pressure created by the piston moving at constant velocity (equivalent to instantaneous piston velocity), this pressure P_B can be obtained from the normal shock wave equation:

$$P_B = P_3\left[1 + \frac{\gamma}{2}\frac{u_{P_K} + \frac{dx}{dt}}{a_3}\left\{\frac{(\gamma+1)}{2}\frac{u_{P_K} + \frac{dx}{dt}}{a_3} + \sqrt{4 + \frac{(\gamma+1)^2\left(u_{P_K} + \frac{dx}{dt}\right)^2}{4a_3^2}}\right\}\right] \qquad (2)$$

The equation of motion of the piston is

$$\frac{M}{gA}\frac{d^2x}{dt^2} = P_4 - P_B \qquad (3)$$

Let us introduce these dimensionless parameters

$$\bar{x} = \frac{x}{x_K}, \quad \bar{P} = \frac{P}{P_3}, \quad \rho = \frac{\rho}{\rho_3}, \quad \bar{T} = \frac{T}{T_3}, \quad \bar{t} = \frac{t}{\tau_K}$$

and substitute Equations (1) and (2) into (3), then we can obtain the equation of motion of the piston during the deceleration process

$$\frac{d^2\bar{x}}{d\bar{t}^2} + \bar{P}_3\left\{1 + \frac{\gamma}{2}\left(\frac{u_3 + \frac{x_K}{\tau_K}\frac{d\bar{x}}{d\bar{t}}}{a_3}\right)\left[\frac{\gamma+1}{2}\left(\frac{u_3 + \frac{x_K}{\tau_K}\frac{d\bar{x}}{d\bar{t}}}{a_3}\right)\right.\right.$$

$$+\sqrt{1+\frac{(\gamma+1)^2\left(u_1+\frac{x_K}{\tau_K}\frac{d\bar{x}}{d\bar{t}}\right)^2}{4a_1^2}}\Bigg]\Bigg\}=\bar{\rho}^{\gamma} \tag{4}$$

When the piston overrushes to reach the peak pressure and then rebounds to point A in Figure 1 (maximum rebounding speeds), the compression waves behind the piston will concentrate into shock waves. After passing point A, the pressure behind the piston is replaced by the pressure produced by the unsteady motion of piston based on the equilibrium state, which is

$$P_2=P_1\left[1+\frac{\gamma-1}{2a_2}\left(\frac{dx}{dt}+u_1\right)\right]^{\frac{2\gamma}{\gamma-1}} \tag{5}$$

Therefore, after passing point A, the equation of motion of the piston should be changed into

$$\frac{d^2\bar{x}}{d\bar{t}^2}+\bar{P}_1\left[1+\frac{\gamma-1}{2a_1}\left(\frac{x_K}{\tau_K}\frac{d\bar{x}}{d\bar{t}}+u_1\right)\right]^{\frac{2\gamma}{\gamma-1}}=\bar{\rho}^{\gamma} \tag{6}$$

The continuity equation of the flow passing through the nozzle is

$$\frac{d(\bar{\rho}\bar{x})}{d\bar{t}}=-\varepsilon\left(1+\frac{\gamma+1}{4}M_1^2\right)\bar{\rho}^{\frac{\gamma+1}{2}} \tag{7}$$

where

$$\varepsilon=\frac{\tau_K}{\tau},\quad \tau_K=\sqrt{\frac{M}{gA}\frac{x_K}{P_1}},\quad \tau=\left(\frac{\gamma+1}{2}\right)^{\frac{\gamma+1}{2(\gamma-1)}}\frac{x_K A}{a_1 A^*}.$$

Equation (4) or Equations (6) and (7) are the equations of motion of the piston and the continuity equation of the flow in the nozzle after the opening of the nozzle in a hypersonic gun tunnel.

When the flow in the nozzle is not considered, $\varepsilon = 0$. At this time we do not have to consider the continuity equation and the $\bar{\rho}$ in Equations (4) and (6) should be replaced by $1/\bar{x}$.

The above is derived under the condition of equal cross-section. For the condition that the driving segment and the driven segment do not have equal cross-sections, we must also consider the

effect of area variation. This effect is primarily shown in the variations of parametrs such as $\bar{P}_{s1}$, $\bar{s}_1$, P_5, x_K and τ_K. It should be pointed out that the mass of the piston has some effect on the acceleration process and consequently on the parameters such x_K, τ_K, etc. Work in this area has been done by several people, it is not going to be discussed here.

III. NUMERICAL COMPUTATION

Starting from the point K at which the piston begins to decelerate, we use the finite difference method to carry out a numerical calculation. For all the parameters before point K, we use the numerical values of those in the shock tube related flow analysis. The parameters at point K are also used as the initial parameters of the computation. The related parameters in region (5) have already taken the effect of the flow in the nozzle into consideration.

When the initial condition is $\bar{\tau} = 0$,

$$\bar{x} = 1, \quad \frac{d\bar{x}}{d\bar{\tau}} = -\frac{\tau_K}{x_K} u_5, \quad \rho = 1 \tag{8}$$

Using the Runge-Kutta method, we change the second order differential equation into a set of first order simultaneous differential equations and use the integration progressing method to obtain the numerical solutions for various initial conditions.

The piston begins to decelerate from point K, it goes through overrush to reach the peak pressure and then rebounds. When it reaches the maximum rebound velocity point A, it begins to decelerate again and then starts the oscillation process. From point K to point A, we use Equations (4) and (7). After point A, we use Equations (6) and (7) to carry out the calculation. In our calculation we assume the gas is an ideal gas and the driving and the driven gases are all air or nitrogen. The ratio of specific heats

is $\gamma = 1.4$ and the initial temperature $T_o = 300°K$.

IV. RESULTS AND DISCUSSIONS

Let us choose that the length of the driven segment is 10 m, and inner diameter is 10 cm. Based on the various initial parameter combinations, listed in Tables 1 and 2, we carried out the computation.

TABLE 1. Initial parameters of open-ended nozzle

1 活塞质量 M (kg)	0.05	0.10	0.20	0.30	0.40	0.50	0.70	1.0	1.5	2.0
2 喷管喉道截面比 A^*/A	0.05	0.10	0.15	0.20	0.25	0.35	0.50			
3 主激波马赫数 M_s	2.0	2.4	2.5	2.8						
4 驱动压力 P_4(kg/cm²)	300	500								

TABLE 2. Initial parameters of closed nozzle (A*/A=0)

5 活塞质量 M(kg)	0.05	0.075	0.10	0.15	0.20	0.25	0.30	0.35
	0.40	0.45	0.50	0.60	0.70	1.0	1.5	2.0
6 主激波马赫数 M_s	2.0	2.4	2.5	2.8				
7 驱动压力 P_4(kg/cm²)	300							

Key: 1--piston mass M (kg); 2--cross-section ratio of throat channel of the nozzle A*/A; 3--Mach number of the main shock wave M_s; 4--driving pressure P_4(Kg/cm^2); 5--mass of the piston M (kg); 6--Mach number of the main shock wave M_s; 7--driving pressure P_4 (kg/cm^2)

The computational results are plotted in Figures 2-4. Figure 2 is the typical situation of the variations of the dimensionless piston trajectory $\bar{x}$ and the dimensionless pressure $\bar{p}$ with the dimensionless time $\bar{t}$ after the piston begins to decelerate from point K for various ratios of the nozzle throat channel A*/A and piston masses M. For their M_s and P_4 values, the results qualitatively have the same trends. Figure 3 shows the relations between the ratio of the peak pressure and the equilibrium pressure $\hat{P}/P_e$ and A*/A as well as M for various M_s values under the conditions of both open and closed nozzles. Figure 4 shows the effect of throat channel ratio on the equilibrium piston mass.

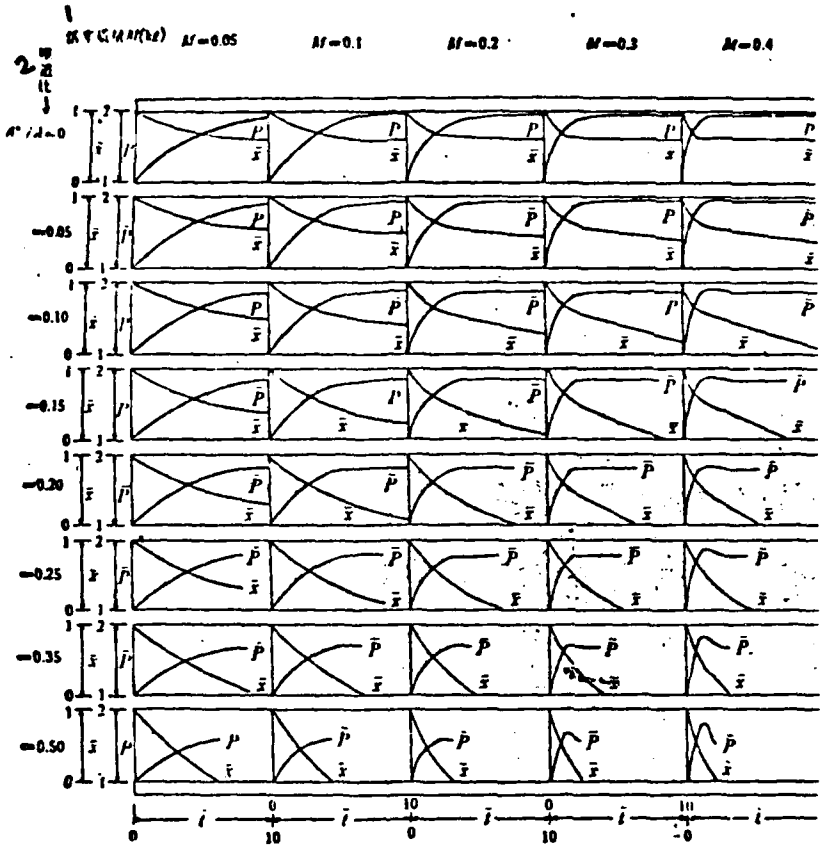

Fig. 2.

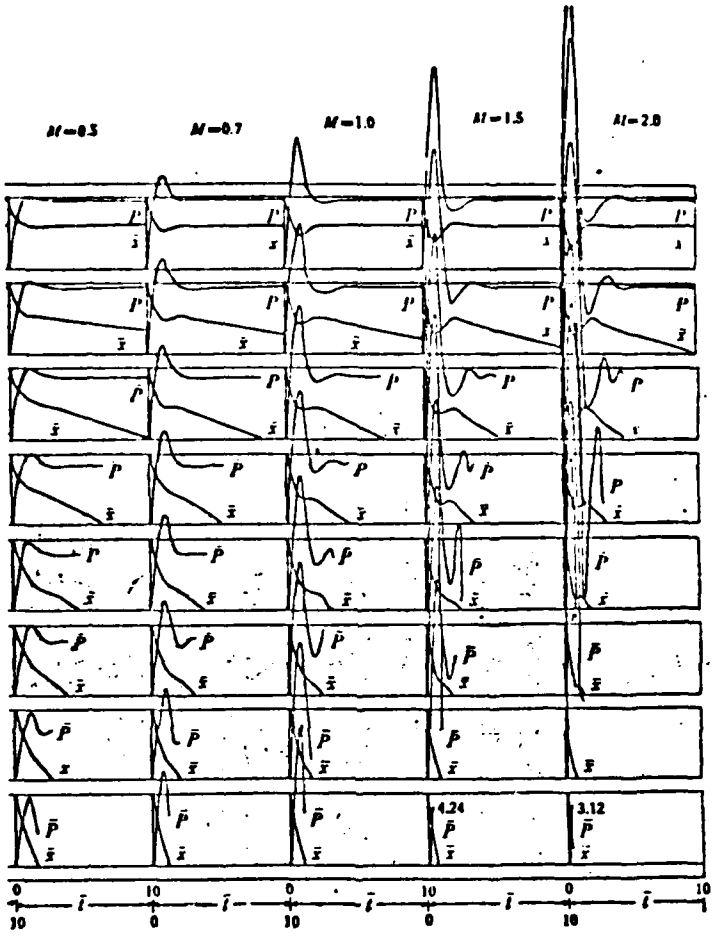

Fig. 2 Cont'd. The typical situation of the variation of the of the dimensionless piston trajectory $\bar{x}$ and the dimensionless pressure $\bar{p}$ with the dimensionless $\bar{t}$ after the piston begins to decelerate from point K under various throat channel ratios of the nozzle A*/A and piston masses M.

Key: 1 - piston mass M(kg); 2 - ration of throat channel.

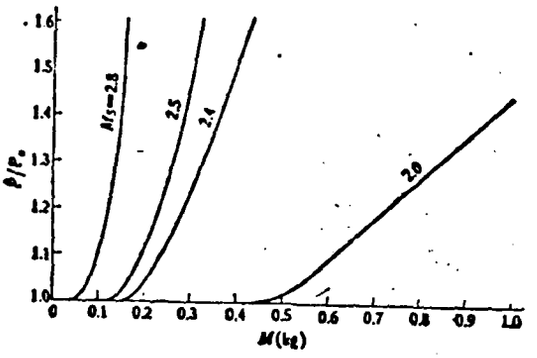

(a) $A^*/A = 0$ $P_0 = 300 kg/cm^2$

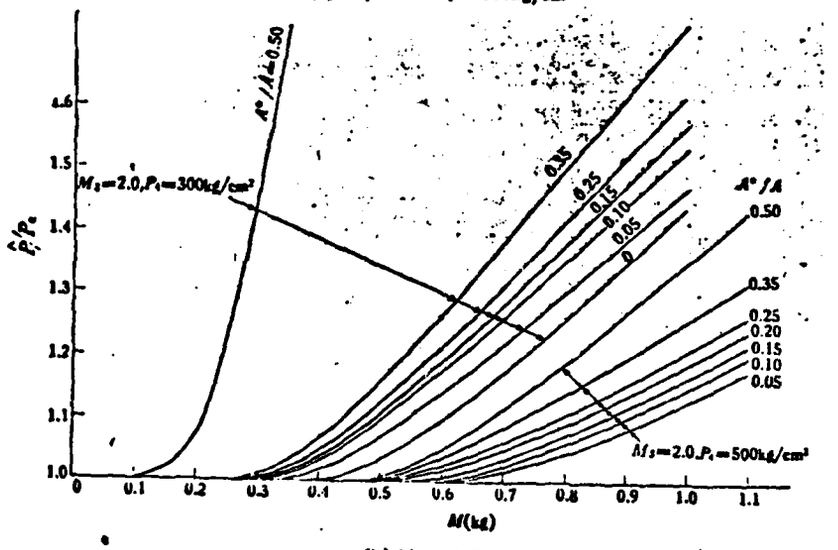

(b) $M_1 = 2.0$

Fig. 3.

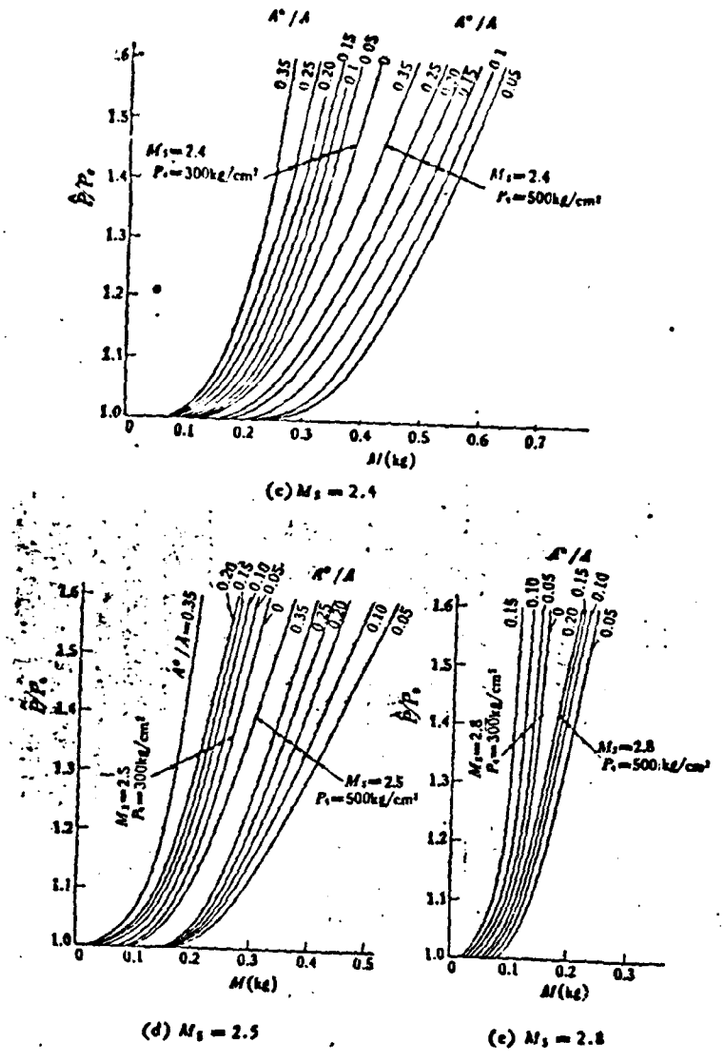

Fig. 3. The relation between the peak pressure and piston mass.

The calculated results, after considering the compression processes after the opening of the nozzle and comparing with those obtained using the conventional analysis of compression processes of the piston on the basis of closed nozzles, indicate the following characteristics:

1. From the variation of $\bar{x}$ with time shown in Figure 2, it was found that the existence of flow in the nozzle has a relaxation effect on the rebound of the piston. This coincides with the results obtained using the microwave technique in [7].

2. From Figure 3, it was found that, regardless whether the nozzle is open or closed, the ratio of the peak pressure and the equilibrium pressure $\hat{P}/P_e$ increases with increasing piston mass M for a given Mach number M_s. For the open nozzle condition, the larger A^*/A is the more serious this situation becomes. Under the condition that there is a flow in the nozzle, due to the effect of gas flow in the stationary chamber on the piston motion on one hand and the main shock wave at the entrance of the nozzle cannot be totally reflected causing the weakening of the reflected shock wave S_r, on the other hand, the deceleration of the piston at point K (i.e., the loss in kinetic energy) becomes smaller. Thus the opening of the nozzle has a relaxing effect on the rebound of the piston which corresponding less makes $\hat{P}/P_e$ become larger.

3. From Figure 4, it is clear that if we take the piston mass at $\hat{P}/P_e = 1.05$ as the equilibrium piston mass M_e and then plot the relations between the equilibrium piston mass S and the ratio of the throat channel of the nozzle for various Mach numbers of the initial shock wave, we can easily see that the effect of the existence of flow in the nozzle on the equilibrium piston mass is apparent. That is for a certain M_s, the larger A^*/A is the smaller M_c becomes.

Besides these, the calculated results also indicate some other regularities in the compression processes of the piston:

1. From Figure 2, it was found that for given M_s and A*/A, the tendency for the piston to oscillate increases as M increases. But the time of exhaustion of the experimental gas flow is independent of M. Of course, the longer A*/A or M_s is, the shorter the exhaustion time is. The calculated results also indicate that for the same A*/A and M, the larger M_s is the higher the tendency of piston oscillation becomes. For the same M_s, the higher P_4 is, the weaker this tendency of oscillating motion becomes with A*/A and M unfixed.

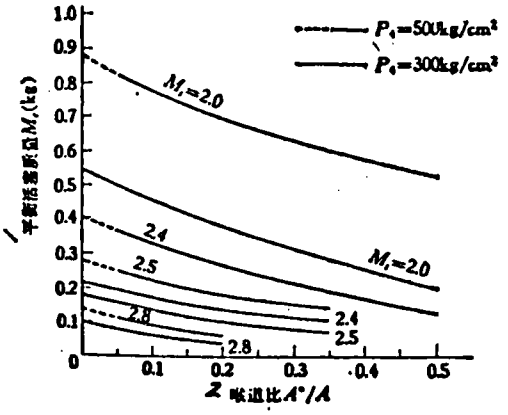

Figure 4. The effect of the throat channel on the equilibrium mass of the piston.

Key: 1--equilibrium piston mass M_e(kg); 2--ratio of throat channel A*/A

2. From Figure 3, it was found that the piston mass which satisfies the $\hat{P}/P_e \leq 1.05$ condition has a finite region which indicates that the requirement of piston mass in the equilibrium piston technique is not very stringent. It is especially so when M_s is lower.

3. As described above, after the piston rebounded beyond point A (Figure 1), the pressure behind the piston P_B should be replaced by Equation (5) instead of Equation (2). However, under the condition that $\hat{P}/P_e \leq 1.10$, the piston almost did not rebound from Figures 2 and 3. Therefore, the replacement is not necessary.

Under the condition that $\hat{P}/P_e \geq 1.10$, if the piston mass is not too large, usually equilibrium can be reached after one rebound. The calculated result for this condition indicates that the use of Equation (5) beyond point A does not make too much difference in the calculated results. If the oscillation motion of the piston is vigorous, then Equation (5) must replace Equation (2) to carry out the calculation.

V. CONCLUSIONS

Similar to other treatment carried out by other people, we established the equation of motion of the piston and the flow equation in the nozzle using the assumption that the compression processes beyond region (5) are isotropic processes. Through calculation and analysis, we discussed the problems related to the overrush, rebound, oscillation, equilibrium running, and peak pressure of the piston after the opening of the nozzle under various conditions of gun tunnel parameters. We compared our results with those obtained using the equilibrium piston motion technique based on closed nozzles and those from experiments. The results indicate that the effect of gun tunnel nozzle flow on the compression processes of the piston is obvious. These results have also received some experimental verification.

In the numerical computation of this work, we have received tremendous assistance from comrade Ho Ni-Tei. We wish to express our thanks here.

REFERENCES

[1] Stalker, R. J., *JFM*, 22 (1965), 675.
[2] Lemke, B., *FPA*, 90 (1960).
[3] Davies, J., Regan, J. L. and Dolman, K. A., ARC CP 982 (1967).
[4] East, R. A. and Pennelegion, L., ARC CP 607 (1962).
[5] Kamimoto, G., Mori, T. and Kimura, T., Proceedings of the 13th Japan National Congress for Applied Mechanics (1963), 185.
[6] 神元五郎ら, 日本航空学会誌, 12, 131(1964).
[7] 神元五郎ら, 日本航空学会誌, 12, 131 (1964).
[8] Knöös, S., *AIAA J.*, 18, 1 (1970).
[9] Evans, C. and Evans, F., *JFM*, 1 (1956), 399.
[10] Winter, D. F. T., *JFM*, 8 (1960), 264.
[11] Courant, R. and Friedrichs, K. O., Supersonic Flow and Shock Waves, Interscience, New York (1948).

PREDICTION OF TURBULENT BOUNDARY LAYER SEPARATION*

Wu Guo-chuan

(Nanjin Aeronautical Institute)

In order to define the velocity distribution which is closely related to the pressure gradient, A. Buri introduced the velocity distribution shape factor Γ [1].

$$\Gamma = \frac{\delta^{**}}{U}\frac{dU}{dx}\left(\frac{U\delta^{**}}{\nu}\right)^{m} \tag{1}$$

where δ^{**} is the momentum thickness $\left(=\int_0^{\delta}\frac{u}{U}\left(1-\frac{u}{U}\right)dy\right)$; U is the velocity in the main flow; u is the velocity in the boundary layer; v is the kinetic viscosity; x is the coordinate along the direction of the flow; m is a constant. When $\Gamma>0$, it corresponds to an accelerating flow. When $\Gamma<0$, it corresponds to a decelerating flow.

In the gas inlet model experiment participated by the author, the result of the measured velocity distribution of model 4 near the separation point in the boundary layer is shown in Figure 1. Based on the measured velocity distribution in the boundary layer, the shape factor was calculated to be $\Gamma = -0.062$. Based on the result measured by Nikuvale, separation began when $\Gamma = 0.06$ or $\Gamma < -0.06$. Let us use $\Gamma = -0.06$ in equation (1) and make $\delta^{**}(U\delta^{**}/\nu)^{m} = Z'$, then we obtain

$$\frac{Z'}{U} = -\frac{0.06}{U'} \tag{2}$$

Finding the derivative of equation (2) with respect to x, we get

*Received on July 21, 1978

$$\frac{d\left(\frac{Z'}{U}\right)}{dx} = \frac{\left(U\frac{dZ'}{dx} - Z'U'\right)}{U^2} = \frac{0.06U''}{U^4} \qquad (3)$$

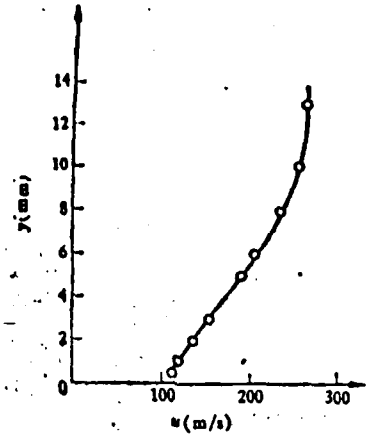

Figure 1. The velocity distribution near the separation point in the boundary layer of gas inlet model number 4.

Buri has assumed that the shear stress on the wall surface in the turbulent boundary layer and the ratio of the displacement thickness to momentum thickness $H(=\delta^*/\delta^{**})$ are functions of the shape factor Γ;

$$\frac{\tau_w}{\rho U^2} = f_1(\Gamma)\Big/\left(\frac{U\delta^{**}}{\nu}\right)^m = f_1(\Gamma)/(R^{**})^m \qquad (4)$$

$$H = \frac{\delta^*}{\delta^{**}} = f_2(\Gamma) \qquad (5)$$

where ρ is the density of the fluid and $R^{**} = U\delta^{**}/\nu$.

Considering equations (4) and (5), we can obtain the following from the momentum equation of the turbulent motion[2]:

$$\frac{d}{dx}[\delta^{**}(R^{**})^m] = F(\Gamma) \qquad (6)$$

where $F(\Gamma) = (1+m)f_1(\Gamma) - [2+m+(1+m)f_2(\Gamma)]\Gamma$. $F(\Gamma)$ is very close to be a straight line (see Figure 2) and it can be expressed as $F(\Gamma) = c - k\Gamma$. Buri used the measured results

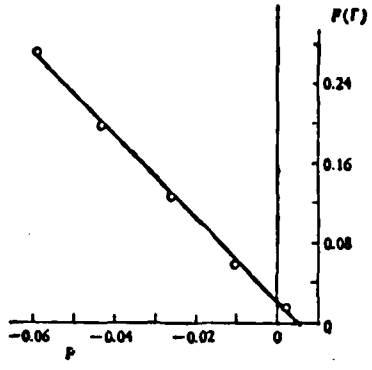

Figure 2. The function $F(\Gamma) = 0.017 - 4.15\Gamma$

of J. Nikuradse together with the assumption that $m = 1/4$ to calculate the parameters c and k. For a decelerating flow, he obtained that $C = 0.017$ and $k = 4.15$[1].

From Figure 2, it was found that when $\Gamma = -0.06$ $F(\Gamma) = 0.26$. Plugging this value into equation (3) and then using equation (2), we can get

$$-d\left(\frac{Z'}{U}\right)/dx = 0.32/U \tag{7}$$

Compare equation (3) with (7), we get

$$-UU''/U'^2 = 5.33 = \sigma \tag{8}$$

The above analysis indicates that when $\sigma > 5.33$, the boundary layer will not separate. But when $\sigma < 5.33$, the boundary layer will separate. $\sigma = 5.33$ then is the condition under which the boundary layer is near separation. From this we can qualitatively determine the conditions under which the boundary layer will not separate and also the shape of the velocity distribution in the main flow.

From equation (8), we know that in order to satisfy the condition that $\sigma > 5.33$ it must be that $U'' > 0$. In other words, the necessary condition for no separation in the boundary layer is

$$U'' > 0 \qquad (9)$$

Therefore, the following conclusions can be reached: 1. If the velocity variation curve in the main flow region after the maximum is concave downward (U"<0) (see Figure 3), the boundary layer separation must occur. 2. If the velocity variation curve in the main flow region is concave upward $(U'' > 0)$, then the boundary layer may separate or it may not separate. When $0 \leqslant \sigma < 5.33$, it separates and when $\sigma > 5.33$ it does not separate. 3. If the boundary layer does not separate, then the velocity variation curve in the main flow region must be concave upward, i.e. $U'' > 0$.

These three conclusions are used to analyse the experimental results obtained from the experiments of the eight gas inlet model the author participated in previously. Figures 4 and 5 are the distribution curves of the theoretical axial M number (neglecting flow loss) in the main flow region of the symmetrical flow surface (the plane slightly below the horizontal dividing plane) in the gas inlet model experiments. The ordinate is the axial M number and the abscissa is the distance z away from the lip.

The axial M number distribution curve reached a maximum very near the lip for model No. 1. After the maximum, the curve apparently is concave upward. Experiment proved that there was no separation region in Model 1 which agrees with the third conclusion discussed above. The distribution curves of the axial M number in the main flow region more or less appear

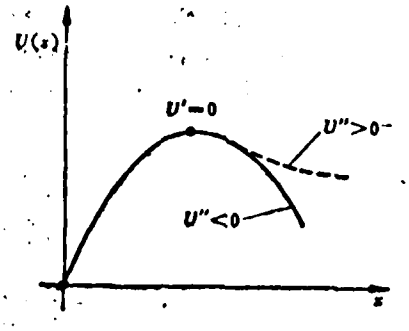

Figure 3. Velocity variation in the main flow region with and without separation in the boundary layer.

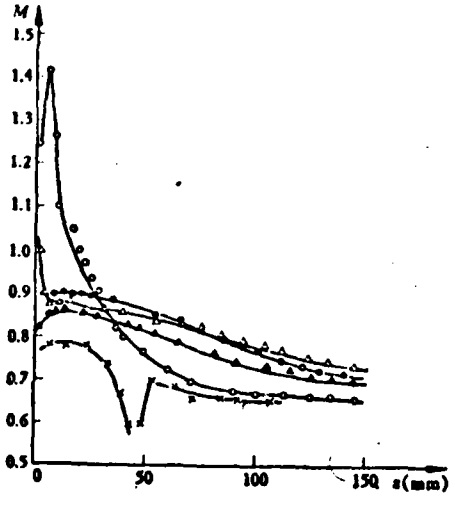

Figure 4.
0 no. 1 x no. 3 ▲ no. 6
● no. 7 ▲ no. 8

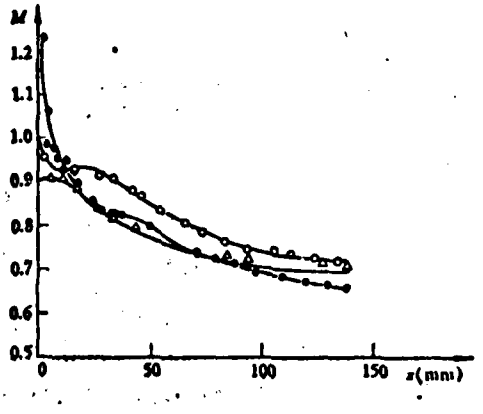

Figure 5.
▲ no. 2 ● no. 4 0 no. 5

to be concave downward. Based on the first conclusion, the boundary layer separation must occur. This was verified experimentally. Comparing the axial M number distribution curves in the main flow region for models 2, 5, 6, 7, and 8, it was found that the curve of model 2 had a very short region

which was concave downward after the maximum. It was immediately followed by an apparent concave upward section. Its separation region is the shortest. The curve for model 8 has a long section concave downward, therefore, the separation region drags for very long. The curves for models 5, 6, and 7 are in the middle. The first portions of the three curves all are concave downward to more or less the same extent. As for the concave upward portion which follows, curve no. 5 appears the earliest and it is also the most apparent. Its separation region also ends the earliest among the three models. The concave upward section in the latter portion of curve no. 7 appears last and it is also the least obvious one. Therefore, its separation region is the longest among the three models. Model 6 is situated between the two mentioned above. The axial M number distribution curve in the main flow region for Model 4 appears to be obviously concave upward in a relatively long region and immediately it appears to be concave downward. The downward region is smaller. It is predicted that the separation region begins later and its range is smaller. Experimental results completely verified the conclusions of the above analyses. The distance between the starting point of the separation region and the lip for model 4 is larger than those for other models. It is 4 m while for other models it is 0.5 - 2.5 m. Curve no. 3 obviously appears to be concave downward in the beginning section. Based on the first conclusion, the boundary layer must separate. Experimental result indeed showed separation.

Table I lists the theoretical analytical predictions and experimental results. It shows more clearly the consistency bewteen theoretical and experimental results.

The above analysis indicates that based on the variation of velocity in the main flow region we can predict whether

Table I

进气道模型编号 5	理论分析估计分离区情况 4	实验结果 1	
		分离区开始点离唇口的距离 x_1(cm) 2	分离区结束点离唇口的距离 x_2(cm) 3
1	无分离 6	0	0
2	2, 5, 6, 7 和 8 号五者中分离区最短 7	1.0	5.2
3	有分离 8	<1.5	5.7
4	分离区开始得迟，范围较小 9	4.0	8.7
5	5, 6 和 7 号三者中分离区最早结束 10	0.5	9.1
6	5, 6 和 7 号三者中居中 11	1.0	9.2
7	5, 6 和 7 号三者中分离区拖得最长 12	1.5	12.3
8	2, 5, 6, 7 和 8 号五者中分离区拖得最长 13	2.4	12.3

Key: 1. Experimental results, 2. The distance from the starting point of the separation region to the lip X_1(cm), 3. The distance from the end point of the separation region to the lip X_2(cm), 4. Predicted situation in the separation region based on theoretical analysis, 5. Model number of gas inlet duct, 6. No separation, 7. Shortest separation region among Model no. 2, 5, 6, 7, and 8, 8. With separation, 9. Separation region starts late and has a small range, 10. Separation region ends the earliest among model no. 5, 6, and 7, 11. The middle one in models 5, 6, and 7, 12. Longest separation region among models 5, 6, and 7, 13. Longest separation region among models 2, 5, 6, 7, and 8.

boundary layer separation will occur or not to a certain extent. It provides basis for the design of gas inlet duct with good flow characteristic and small stagnation pressure loss. Or, it can predict the quality of the gas inlet duct already designed. It can be envisioned that the velocity variation in the main flow region can first be defined during the design in order to select a variation which corresponds to a flow with good behavior and no boundary layer separation. The dimensions and the geometric shape of the cross-section can then be determined based on the velocity variation.

The necessary condition for no separation in the turbulent boundary layer obtained in this paper is actually not related to the parameters associated with the gas inlet duct itself.

Therefore, this conclusion is not only applicable to gas inlet ducts, it also applies to the turbulent flow inside compressors and cascades.

References

[1] Schlichting, H., Boundary Layer Theory, McGraw Hill Book Company, Inc., N.Y. (1960).

[2] Лойцянский, Л. Г., Механика жидкости и газа, Государственное издательство, Москва (1957).


ATE
LMED
8